Effects of Polarization Reversal on Localized-Absorption Characteristics of Electron Cyclotron Wave in Bounded Plasmas

doi: 10.1063/1.2103547

Effects of polarization reversal on localized-absorption characteristics of electron cyclotron wave in bounded plasmas

K. Takahashi, T. Kaneko, and R. Hatakeyama
Department of Electronic Engineering, Tohoku University, Sendai 980-8579, Japan

(Received 25 May 2005; accepted 12 September 2005; published online 19 October 2005)

Propagation and absorption of electron cyclotron wave are investigated for the case in which a left-hand polarized wave (LHPW) is selectively launched in inhomogeneously magnetized and bounded plasmas. The LHPW is observed to be unexpectedly and sharply absorbed near the electron cyclotron resonance point. The unexpected absorption of the LHPW is clarified to be caused by a polarization reversal from the LHPW to a right-hand polarized wave. It is found that the polarization reversal point dominates the absorption region of the electron cyclotron wave, which is observed to be changed by controlling the plasma radius, i.e., radial boundary condition. These phenomena can be well explained in terms of the dispersion relation in bounded plasmas. © *2005 American Institute of Physics*. [DOI: 10.1063/1.2103547]

I. INTRODUCTION

Electron cyclotron waves are important plasma waves in the fields of basic plasma physics, plasma application, thermonuclear fusion, and so on. Localized electron cyclotron resonance (ECR) heating has been hoped to be the most effective method for the formation of thermal transport barrier in tandem-mirror devices,[1–3] where strong electron heating in the perpendicular direction against magnetic-field lines are demanded. Although sufficient confinement has not been attained by using ECR in the devices so far, the heated hot electrons can efficiently ionize neutral gases and produce ions. Making use of this knowledge, ECR is utilized for ion production in an ion engine system for propulsion of satellites,[4] and ion beam sources for various experiments of atomic physics, nuclear physics, and so on.[5,6] The wave propagation and absorption play important roles in these applications. It was reported that an absorption region of the wave power affects the efficiency of the electron heating in an ECR discharge, where the localized wave absorption promotes the high electron temperature.[7] Although the localized wave absorption is considered to be necessary for efficient and strong electron heating and yield efficient ion production, the Doppler shift effect by high energy electrons was reported to expand the resonance region, i.e., wave absorption region is broadened in an ECR discharge.[8] Thus, wave characteristics with more localized resonance region are expected to yield stronger electron heating and more efficient ion production. When the wave propagations in the ECR discharges utilized for the ion thrusters and the beam sources are taken up, on the other hand, the effects of boundary conditions should be taken into account because the wavelength of the microwave is comparable with the length or diameter of plasmas and devices.

From the viewpoint of plasma physics, a right-hand polarized wave (RHPW) has been investigated for a long time,[8–11] because the RHPW is efficiently absorbed near the ECR point. On the other hand, a left-hand polarized wave (LHPW) has been known to be absorbed at $\omega=\omega_{pe}$ due to Landau damping,[12] where $\omega/2\pi$ and $\omega_{pe}/2\pi$ are wave and electron plasma frequencies, respectively. Moreover, recent experimental results demonstrated that the LHPW in a bounded plasma is also unexpectedly absorbed near the ECR point just like the RHPW.[13–15] In order to explain the unexpected absorption of the LHPW, a polarization reversal from the LHPW to the RHPW was theoretically suggested[16] and experimentally investigated for the case of a partially filled plasma-waveguide in an ECR discharge.[14] But, the polarization reversal has not been clearly observed and its physical mechanism has not been clarified. In our previous paper,[15] the experimental results demonstrated that the absorption region of the LHPW is more localized than that of the RHPW. Although the mechanism has not been clarified yet, we believe that the localized LHPW absorption can lead to the localized and strong electron heating, because the wave electric-field strength of the LHPW at the ECR point is larger than that of the RHPW, which starts to damp farther from the ECR point compared with the LHPW. Therefore, it is very important to understand the absorption mechanisms and characteristics of the LHPW near the ECR point.

Based on these backgrounds, the purposes of the present work are to clarify the absorption mechanisms and to understand the absorption characteristics of the LHPW near the ECR point. In this paper, the first observation of the polarization reversal and absorption mechanisms of the LHPW due to the polarization reversal in bounded plasmas are reported. The polarization reversal is found to be explained by the dispersion relation including the effect of a radial boundary condition, which fixes a wave number perpendicular to the magnetic-field lines. Its effect yields a different dispersion relation and wave polarizations from that in unbounded plasmas. A brief result of this work has been reported earlier.[17] In Sec. II, an experimental setup is described. A theory of dispersion relation is mentioned in Sec. III. Experimental results are presented in Sec. IV. We discuss the results in Sec. V, and conclusions are given in Sec. VI.

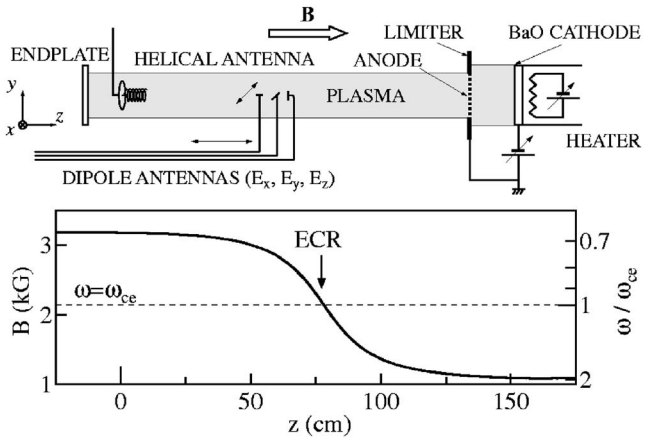

FIG. 1. Schematic of experimental apparatus and static magnetic-field configuration.

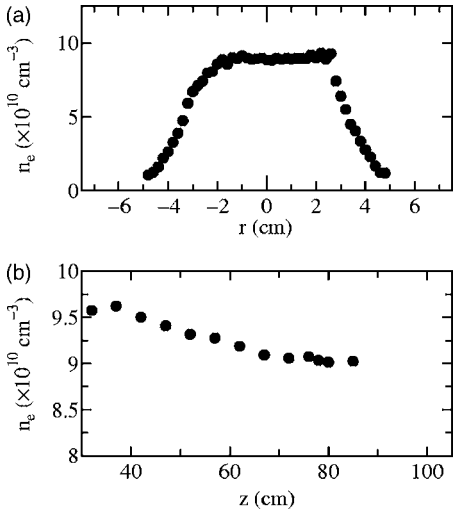

FIG. 2. (a) Radial and (b) axial profiles of electron density measured by the Langumuir probes at (a) $z=78$ cm and (b) $r=0$ cm.

II. EXPERIMENTAL SETUP

Experiments are performed in the Q_T-Upgrade Machine of Tohoku University as shown in Fig. 1, which is a linear device with vacuum chamber about 450 cm in length and 20.8 cm in diameter. The inhomogeneous magnetic field B presented in Fig. 1 is applied by two parties of solenoidal coils. A coaxial bounded plasma with peripheral vacuum layer is produced by a direct current discharge between a barium oxide (BaO) cathode and a tungsten mesh anode in low pressure argon gas (90 mPa). The plasma column is terminated by a glass endplate located on the opposite side of the plasma source. The formation of clear boundary between the plasma and the vacuum layer is realized by using a limiter, which is located just in front of a tungsten mesh anode and also enables the plasma radius r_p to be controlled in the range of 2.5–4 cm. Radially and axially movable Langmuir probes are set in order to measure plasma parameters and their radial and axial profiles. The typical electron density and temperature at the radial center of the plasma column are $n_e \simeq 9\times 10^{10}$ cm^{-3} and $T_e=3$ eV at $z=78$ cm, where $z=0$ cm is defined as an axial position of a microwave exciter which is described below. Figures 2(a) and 2(b) show the radial and the axial profiles of electron density n_e for $r_p=4$ cm, respectively. It is found in Fig. 2(a) that the radial profile is uniform within the range of ±3 cm, which is in agreement with the expected radius at $z=78$ cm. That is to say, the plasma radius is narrowed along the inhomogeneous magnetic-field lines. In addition, it is confirmed that the electron density is not zero at the edge of the plasma column, i.e., the outside of the limiter, which is caused by the radial diffusion. Figure 2(b) indicates that the electron density in the downstream region slightly increases compared with that in the upstream region because of the reduction of the cross section of the plasma column.

A microwave (6 GHz, 150 mW) is selectively launched toward the ECR point ($B=2.14$ kG, $z=78$ cm) as the LHPW in the high magnetic-field region by a helical antenna ($z=0$ cm). The helical antenna is designed to operate at 6 GHz with the theory in Ref. 18. The diameter of the helix, the axial length, the number of turns, and the diameter of the ground plane behind the helix are 1.6 cm, 12 cm, 10 turns, and 3.75 cm, respectively. When the magnetic-field direction is changed, it was reported that not the LHPW but the RHPW can be excited.[15] The wave patterns are obtained with an interference method by using a mixer through movable balanced dipole antennas with folded balun, which can receive each of the components of the wave electric field, i.e., E_x, E_y, and E_z, respectively, and are terminated with 50 Ω lines. In order to protect the antennas from the thermal damage, these are covered with ceramics. The length of the dipole antennas is selected as 1.8 cm according to the fact that the antennas have the best sensitivity for the case of this length. Here, we mention that the helical antenna is experimentally confirmed not to generate harmonics, which is considered to generate the short wavelength components in the interference method. In addition, shifting the phase of a received signal by using a phase shifter, which is inserted between the dipole antennas and the mixer, can realize measurements of time-series of electric field, because the interferometric wave pattern signifies a snapshot of the electric-field structure at a certain time. Moreover, spatial profiles of the wave power P_x, P_y, and P_z are measured with a power meter.

III. THEORY

A. Dispersion relation in bounded plasmas

We consider the azimuthally and radially uniform plasma column, since the radial profile of electron density is almost uniform as shown in Fig. 2(a). A dielectric tensor $\mathbf{K}$ in cold plasmas is given by

$$\frac{\omega^2}{c^2}\mathbf{K}=\begin{pmatrix}\kappa_1 & \kappa_2 & 0\\ -\kappa_2 & \kappa_1 & 0\\ 0 & 0 & \kappa_3\end{pmatrix}, \tag{1}$$

with κ_1, κ_2, and κ_3 defined by

$$\frac{c^2}{\omega^2}\kappa_1 = 1 - \sum_j \frac{\omega_{pj}^2}{\omega^2 - \omega_{cj}^2},$$

$$i\frac{c^2}{\omega^2}\kappa_2 = \sum_j \frac{\epsilon_j \omega_{cj}\omega_{pj}^2}{\omega(\omega^2 - \omega_{cj}^2)},$$

$$\frac{c^2}{\omega^2}\kappa_3 = 1 - \sum_j \frac{\omega_{pj}^2}{\omega^2},$$

where ω_{pj}, ω_{cj}, and ϵ_j are the plasma frequency, the cyclotron frequency, and the sign of the charge for species j. The terms related to ion motions can be neglected in the case of $\omega \gg \omega_{pi}, \omega_{ci}$, where ω_{pi} and ω_{ci} are the ion plasma and cyclotron frequencies. A dispersion relation of electromagnetic waves in bounded plasmas is derived by using the Maxwell equations as[19]

$$(\gamma^2 + \kappa_2^2 + \gamma k_\perp^2)\kappa_3 + k_\perp^2[\kappa_1(\gamma + k_\perp^2) - \kappa_2^2] = 0, \tag{2}$$

where $\gamma \equiv k_\parallel^2 - \kappa_1$, $k_\parallel$ and $k_\perp$ are the wave numbers parallel and perpendicular to a static magnetic field **B**, respectively. The electric fields are assumed to propagate toward the z direction, so the wave fields with azimuthal mode number m can be represented by

$$\mathbf{E} = \mathbf{E}(r)\exp[i(k_\parallel z + m\theta - \omega t)], \tag{3}$$

where the components of the electric-field vector are derived as

$$E_z(r) = \frac{\omega\kappa_1\beta A}{k_\parallel\kappa_2\kappa_3} J_m(k_\perp r), \tag{4}$$

$$E_r(r) = \frac{i\omega\delta A}{\kappa_2 k_\perp} J'_m(k_\perp r) - \frac{m\omega A}{r k_\perp^2} J_m(k_\perp r), \tag{5}$$

$$E_\theta(r) = -\frac{m\omega\delta A}{r\kappa_2 k_\perp^2} J_m(k_\perp r) - \frac{i\omega A}{k_\perp} J'_m(k_\perp r), \tag{6}$$

where $\beta \equiv \gamma - \kappa_2^2/\kappa_1 + k_\perp^2$, $\delta \equiv \gamma + k_\perp^2$, and A and J_m are an amplitude constant and Bessel function of order m, respectively. Here, E_r and E_θ in cylindrical coordinates correspond to experimentally obtained E_x and E_y in rectangular coordinates. In general, the perpendicular wave number $k_\perp$ is determined by radial boundary conditions. Although the parallel wave number $k_\parallel$ is also affected by axial boundary conditions, the parallel wavelength is much less than the axial length of the plasma column in our experimental configurations, which allows us to neglect its effects.

It is well known that the wave polarization plays important roles in cyclotron resonance phenomena. The above dispersion relation and electric-field components derive a polarization index S as

$$S \equiv \frac{|E_r + iE_\theta|}{|E_r - iE_\theta|}. \tag{7}$$

Here, $0 < S < 1$ and $1 < S < \infty$ represent right-handed and left-handed polarizations, and $S=0$, $S=1$, and $S=\infty$ correspond to circularly right-handed, linear, and circularly left-handed polarizations, respectively. We mention that the wave polarization can become both right-handed and left-handed following Eq. (7), which is determined by Eqs. (5) and (6) derived from the solution of Eq. (2), and depends on the plasma parameters, i.e., electron density, magnetic-field strength, and so on.

B. Effects of inhomogeneous *B*-field configuration

The wave frequency $\omega/2\pi$ is constant and the static magnetic-field strength B is varied when we consider the spatial wave propagation in the z direction. Therefore, not wave frequency $\omega/2\pi$ but the magnetic-field strength $B(z)$, i.e., electron cyclotron frequency $\omega_{ce}/2\pi$, has to be regarded as a variable in calculating the dispersion relation given by Eq. (2) for an inhomogeneous magnetic-field configuration. In addition, the inhomogeneity of some plasma parameters due to the magnetic-field configuration should be considered. The first is an axial profile of the electron density $n_e(z)$. We define $n_e(z_0) = n_{e0}$ and $B(z_0) = B_0$ at a certain axial point $z = z_0$. We neglect the electron and ion magnetic-mirror reflection caused by $-\mu\nabla_\parallel B$ force in the converging magnetic-field configuration toward the helical antenna, where μ is the magnetic moment. In addition, we assume that the perpendicular component of electron initial velocity is much less than the parallel one, i.e., $v_{\perp 0}^2/v_{\parallel 0}^2 \ll 1$, because the electrons are accelerated along the magnetic-field lines for the case of the DC discharge. The axial conservation principles of charged particle flux, energy, magnetic moment, and magnetic flux derive a local electron density $n_e(z)$ as

$$n_e(z) = \frac{v_{\parallel 0}}{\sqrt{v_{\parallel 0}^2 + (1 - B(z)/B_0)v_\perp^2}} \frac{B(z)}{B_0} n_{e0} \simeq \frac{B(z)}{B_0} n_{e0}. \tag{8}$$

The local electron density is not simply proportional to B as shown in Fig. 2(b), because the experiments are done in the collisional plasma. However, it is actually found that the electron density increases with an increase in B, which implies a validity of Eq. (8) to some extent. We assume the ideal configuration in order to simplify the calculation of the dispersion relation in Eq. (2).

The second is the perpendicular wave number $k_\perp$, which is determined by the radial boundary conditions at the conducting vacuum wall and between the plasma and the peripheral vacuum layer for the case of partially filled plasma waveguides. In our experimental configuration, since the helical antenna can excite the transverse electric-field mode in empty waveguides, the axial component E_z of wave electric field is absent in the peripheral vacuum layer. In the plasma column, on the other hand, E_z has a finite value. Consequently, the boundary equation can be derived as $E_z = 0$, i.e., $J_m(k_\perp a) = 0$, between the plasma and the vacuum layer $(r = a)$. The radial boundary position is axially varied along the curved magnetic-field lines. When the perpendicular wave number at $z = z_0$ is defined as $k_{\perp 0}$, the local perpendicular wave number $k_\perp(z)$ can be written as

$$k_\perp(z) = \sqrt{\frac{B(z)}{B_0}} k_{\perp 0}. \tag{9}$$

The radial boundary position $r = a$ cannot be exactly identified because of the finite electron density around the edge of

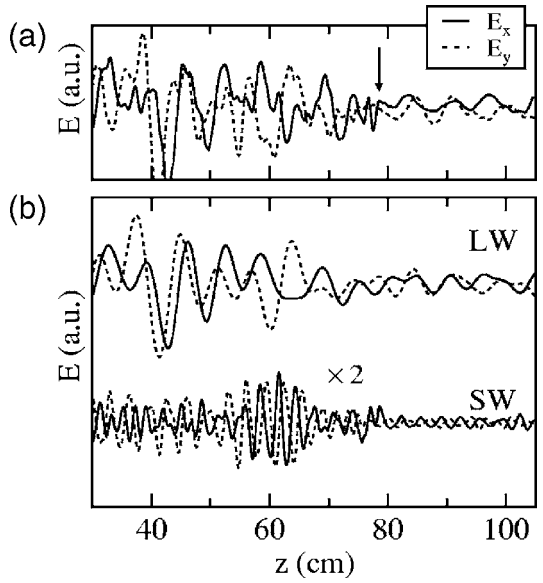

FIG. 3. (a) Interferometric wave pattern of E_x (solid line) and E_y (dashed line). (b) Long (LW) and short (SW) wavelength components decomposed from the wave pattern in (a).

the plasma column as shown in Fig. 2(a). Thus, we use the measured perpendicular wave number in the plasma column as $k_{\perp 0}$.

IV. EXPERIMENTAL RESULTS

Figures 3(a) and 3(b) show the interferometric wave patterns of E_x (solid line) and E_y (dashed line) at the radial center of the plasma column for $r_p=3$ cm, and the long (LW) and short (SW) wavelength components decomposed from the wave patterns of Fig. 3(a) by using Fourier analysis, respectively. Here, the solid arrow in Fig. 3(a) denotes the ECR point and the digital high- and low-pass filters with the border at $k_\parallel/2\pi=0.2$ cm^{-1}, which corresponds to the wave number of 6 GHz microwave in vacuum, are used to decompose to the LW and the SW. Figure 3(a) indicates that the launched LHPW is absorbed near the ECR point just like the RHPW. It is noted in Fig. 3(b) that the LW damps and the SW grows around $z=60$ cm. Moreover, it is obviously observed that the phase difference of E_x to E_y for the LW and the SW is oppositely shifted. Therefore, we plot the axial profiles of the electric-field vector of the LW and the SW in Figs. 4(a) and 4(b), respectively, which are obtained from the wave patterns of E_x and E_y. Figure 4 signifies that the polarization of the SW is opposite to that of the LW. As the wave propagates in the direction of the arrows shown as $k_\parallel$ in Fig. 4, it is identified that the polarization of the LW and the SW are left- and right-handed, respectively. In addition, time-series of electric-field vector of the LW and the SW are directly measured as plotted in Figs. 5(a) and 5(b) in order to determine the polarization direction of the LW and the SW. Here, the symbol T is the period of 6 GHz microwave and the solid circles with arrow denote the rotating directions of the observed vector. It is precisely observed that the polarizations of the LW and the SW are left- and right-handed, respectively. The above-mentioned results lead to a clear-cut

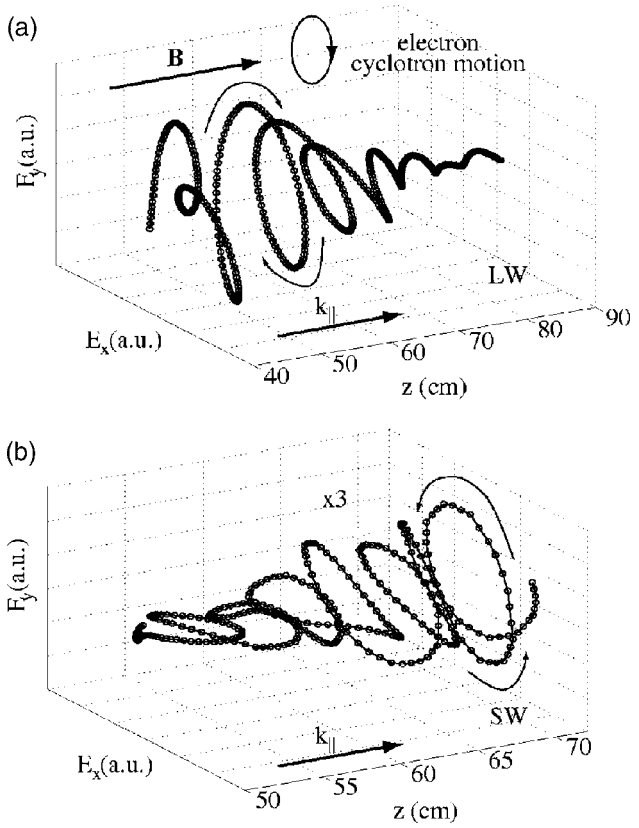

FIG. 4. Axial profiles of electric-field vector of (a) the LW and (b) the SW in transverse plane against the magnetic-field lines.

observation that the LHPW damps and the RHPW grows before the ECR point, that is to say, it is verified that the polarization reversal from the LHPW to the RHPW occurs. As a result, it is disclosed that the launched LHPW is absorbed near the ECR point.

Figure 6 gives the decomposed RHPW components with the plasma radius r_p as a parameter. The polarization reversal point is defined as an axial point where the RHPW has a maximum amplitude as indicated by solid arrows. It is found that the polarization reversal point gradually shifts to the

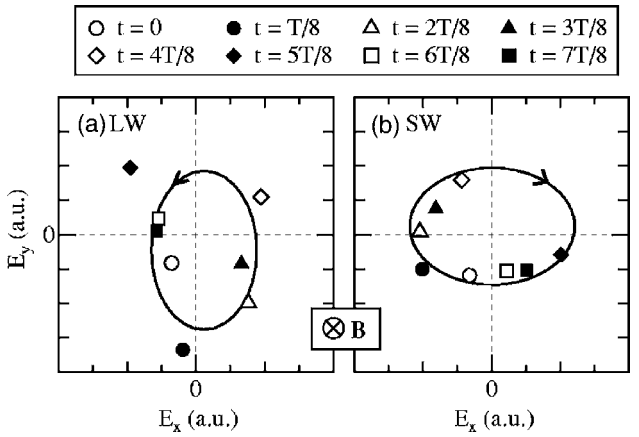

FIG. 5. Time-series of the electric-field vector in transverse plane against the magnetic-field lines of (a) the LW and (b) the SW.

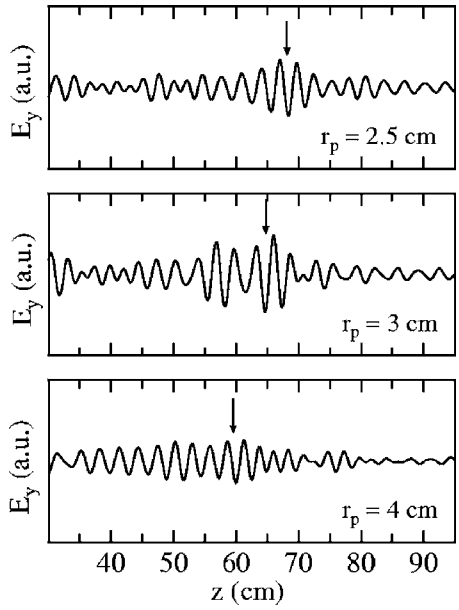

FIG. 6. The RHPW components included in the observed wave patterns with plasma radius r_p as a parameter.

upper region of the wave propagation with an increase in r_p. The polarization reversal is expected to be affected by the radial boundary.

The axial profiles of received wave power P_y (solid lines) for the same conditions as Fig. 6 are presented in Fig. 7 with r_p as a parameter. For each plasma radius, it is found that the wave power is absorbed near the ECR point, where we direct our attention to the absorption region of the wave power. Derivatives $-dP_y/dz$ are presented as dashed lines in Fig. 7 for estimation of absorption region, where $-dP_y/dz$ means absorption degree of the wave power. Figure 7 denotes that the absorption region moves to the upper region of the wave propagation and is broadened with an increase in r_p.

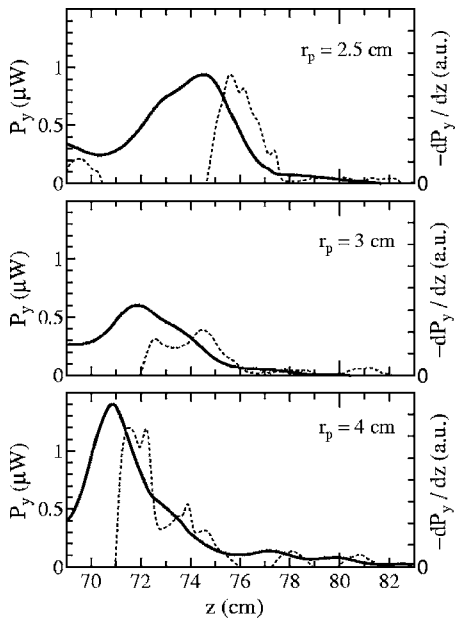

FIG. 7. Axial profile of received microwave power P_y (solid line) and derivatives $-dP_y/dz$ (dashed line) with r_p as a parameter.

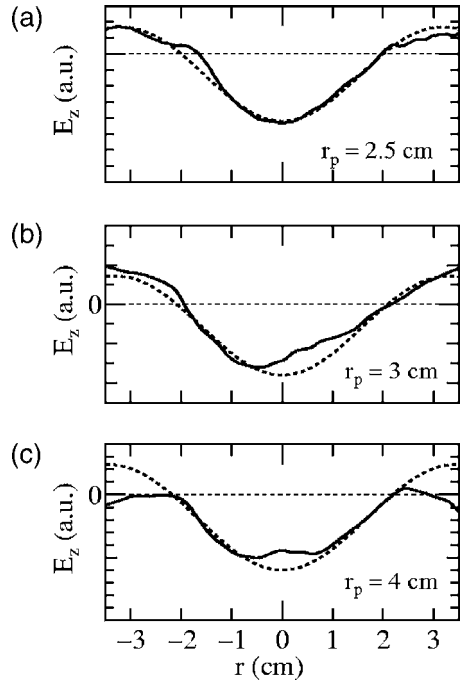

FIG. 8. Radial profile of E_z (solid line) and the calculated Bessel function of order zero (dashed line) with r_p as a parameter.

The results shown in Figs. 6 and 7 signify that the absorption region becomes more localized when the polarization reversal occurs more closely to the ECR point, and that the polarization reversal point is dominated by the plasma radius, i.e., the radial boundary condition. The plasma column is expected to affect the perpendicular wave number $k_\perp$, which is determined by the radial boundary conditions. Therefore, the radial profile of E_z, which gives the azimuthal mode number m and the perpendicular wave number $k_\perp$ according to Eq. (4), is measured for each plasma radius. The measured radial profiles of E_z are presented in Fig. 8 as solid lines. The symmetries of the obtained radial profiles of E_z for each r_p give $m=0$ and allow us to fit the obtained profiles by the Bessel function of order zero. The dashed lines in Fig. 8 are curves fitting the radial profile of E_z with the Bessel function $J_0(k_\perp r)$ of order zero, where $k_\perp=1.20$, 1.15, and 1.1 cm^{-1} for $r_p=2.5$, 3, and 4 cm, respectively. It is clarified that the perpendicular wave number $k_\perp$ varies when the plasma radius r_p is changed. The mechanisms of the results presented in this section are discussed in Sec. V based on the perpendicular wave numbers obtained from Fig. 8.

V. DISCUSSION

In this section, we discuss three observed phenomena. The first is related to a mechanism of the polarization reversal, which is described in Figs. 3–5. The experimentally obtained dispersion relation of the LHPW and the RHPW components, i.e., the LW in the high magnetic-field region and the SW growing near the ECR point in Fig. 3(b), are plotted in Fig. 9(a) as closed and open squares, respectively. The

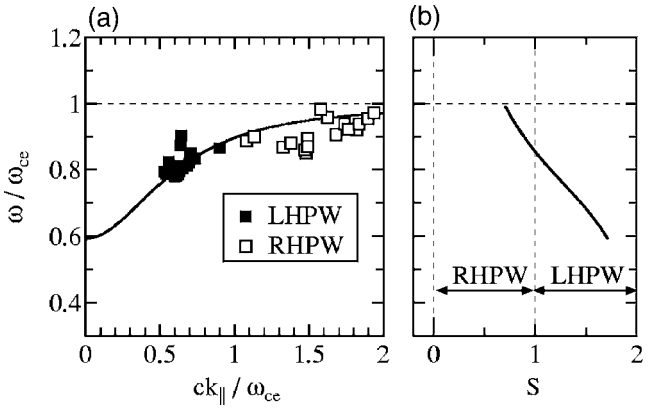

FIG. 9. (a) Calculated dispersion relation (solid line) in bounded plasmas together with the experimental one of the LHPW (closed square) in the high magnetic-field region and the RHPW near the ECR point (open square). (b) Calculated polarization index S corresponding to the dispersion relation in (a).

obtained dispersion relations of both the LHPW and the RHPW are in good agreement with the theoretical dispersion relation (solid line) given by Eq. (2) for the case of experimentally obtained $k_{\perp 0}=1.15\ \mathrm{cm}^{-1}$ and $m=0$ at $z=40$ cm. Figure 9(b) indicates the theoretical polarization index S corresponding to the dispersion curve shown in Fig. 9(a). The value of S is larger than unity in the range of $\omega/\omega_{ce}<0.85$, that is to say, the wave polarization is left-handed in the high magnetic-field region. As the wave approaches toward the ECR point ($\omega/\omega_{ce}=1$), S becomes smaller than unity. It is proved that the polarization reversal from the LHPW to the RHPW can be explained by the dispersion relation including the effect of $k_{\perp}$, i.e., radial boundary, and the effects of the inhomogeneous magnetic-field configuration. Although the helical antenna can in principle excite the left-hand circularly polarized wave, it is conjectured that the restriction of the radial boundary, i.e., dispersion relation in bounded plasmas, makes the wave polarization left-elliptic-handed.

The second is related to the growth of the RHPW near the ECR point as shown in Fig. 3(b). In Sec. IV, we insisted that the growth is caused by the polarization reversal from the LHPW, based on the result that the growth occurs simultaneously with the damping of the LHPW. However, we should now discuss the relation between the wave amplitude E and the group velocity v_g, since it is possible that the wave amplitude grows due to a decrease in v_g, which can be derived from the energy flux conservation ($v_g E^2=\mathrm{const}$). That is to say, there is doubt that the RHPW around $z\simeq 60$ cm is derived from the noiselike SW component around $z=40$ cm. The axial profile of the electric-field amplitude E_{cal} (solid line) calculated from the dispersion relation in Fig. 9(a) under the restriction of the energy flux conservation is presented in Fig. 10 together with the experimental electric-field strength E_{exp} (open square) obtained from the wave pattern in Fig. 3(b). The theoretical curve certainly shows that the electric-field enhancement could occur near the ECR point due to the strong reduction of v_g. On the other hand, the experimentally observed enhancement of the RHPW occurs on the high magnetic-field side enough ahead of the theoretical position of the growth. Therefore, there is no possibility that the observed growth of the RHPW is due to the reduction of v_g. We assert again that it is caused by the polarization reversal obeying the dispersion curve in Fig. 9(a).

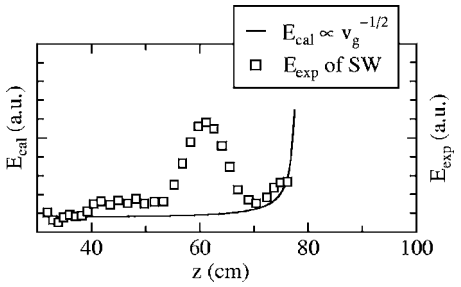

FIG. 10. Theoretical electric-field strength E_{cal} (solid line) obtained from the energy flux conservation for the case of the dispersion relation in Fig. 9(a) and experimentally obtained electric-field strength E_{exp} (open squares) of the SW in Fig. 3(b).

Finally, we discuss the effects of the plasma radius on the polarization reversal point and the wave absorption region in Figs. 6 and 7. The measured perpendicular wave number at $z=40$ cm are $k_{\perp}=1.20$, 1.15, and 1.10 cm^{-1} for $r_p=2.5$, 3, and 4 cm as shown in Fig. 8, respectively, and it is confirmed that the wave is affected by the radial boundary. By using these values, the calculations of the dispersion relation given by Eq. (2) are carried out. The calculated dispersion relation and polarization index S for $r_p=2.5$, 3, and 4 cm are presented in Figs. 11(a) and 11(b) as dashed, solid, and dotted lines, respectively. It is found that the parallel wave number $k_{\parallel}$ becomes larger with an increase in r_p in Fig. 11(a). Then, our attention is focused on the polarization index S for each plasma radius in Fig. 11(b). It is noticed that ω/ω_{ce} at the polarization reversal point becomes smaller with an increase in r_p, i.e., is shifted to the high magnetic-field region. Here, the polarization reversal point stands for the position where the polarization index is converted from $S>1$ into $S<1$. The dependency of the polarization reversal point on r_p is consistent with the observed one in Fig. 6. We now consider the relation between the polarization reversal point and the absorption region. When the polarization reversal occurs in a higher magnetic-field region for larger r_p, the wave has a larger $k_{\parallel}$ as shown in Fig. 11(a). Then, the

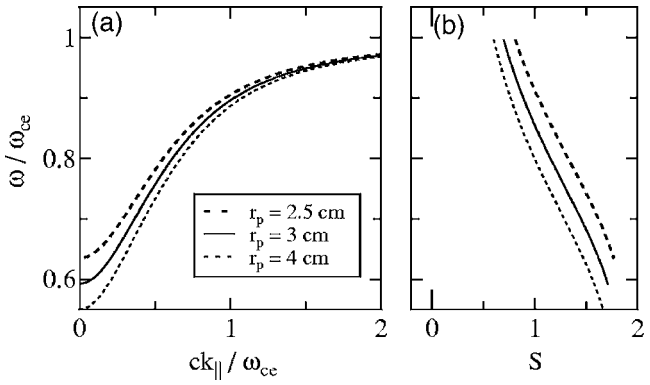

FIG. 11. Calculated dispersion relation and polarization index for the case of $r_p=2.5$ (dashed line), 3 (solid line), and 4 cm (dotted line).

Doppler shift effect acts more conspicuously and the start position of the wave absorption moves to the high magnetic-field region, because the electron cyclotron resonance condition of the wave can be described as $\omega - k_{\parallel} v_e = \omega_{ce}$ and electron temperature is actually finite, where v_e is the axial velocity of electrons and $k_{\parallel} v_e$ is negative. Thereby, the absorption region moves to the high magnetic-field region and is broadened with an increase in r_p. The above-mentioned fact indicates that the LHPW with large $k_{\perp}$ can yield more localized electron heating due to the localized wave absorption.

VI. CONCLUSION

Propagation and absorption of electromagnetic waves in the range of electron cyclotron resonance (ECR) frequency are experimentally and theoretically investigated for the case in which the left-hand polarized wave (LHPW) is selectively launched into the inhomogeneously magnetized and bounded plasmas with the helical antenna. It is for the first time demonstrated that the polarization reversal from the LHPW to the right-hand polarized wave (RHPW) occurs near the ECR point. The polarization reversal can be explained by the dispersion relation including the effects of the radial boundary and inhomogeneous magnetic-field configuration. In addition, the effects of the radial boundary on the wave propagation and absorption are experimentally examined by changing the plasma column radius, namely, perpendicular wave number against the static magnetic-field lines. As a result, the polarization reversal point gets closer to ECR point and the wave absorption region becomes more localized with a decrease in the plasma radius. The phenomena can also be understood theoretically by the dispersion relation in bounded plasmas, indicating that the existence of the radial boundary localizes the absorption region of electron cyclotron wave in laboratory plasmas. The localized absorption of the LHPW could be utilized for localized and strong electron heating, and the resultant efficient ion production.

ACKNOWLEDGMENTS

The authors are indebted to H. Ishida for his technical assistance. We also express our gratitude to Professor K. Sawaya for his useful comments.

This work was supported by a Grant-in-Aid for Scientific Research from the Ministry of Education, Culture, Sports, Science and Technology, Japan. The work was also supported by Research Fellowships of the Japan Society for the Promotion of Science for Young Scientists.

[1] K. Yatsu, L. G. Bruskin, T. Cho, M. Hamada, M. Hirata, H. Hojo, M. Ichimura, K. Ishii, A. Itakura, I. Katanuma, Y. Kiwamoto, J. Kohagura, S. Kubota, A. Mase, Y. Nakashima, T. Saito, Y. Sakamoto, T. Tamano, Y. Tatematsu, T. Tokuzawa, and M. Yoshikawa, Nucl. Fusion **39**, 1707 (1999).
[2] T. Kaneko, R. Hatakeyama, and N. Sato, Phys. Rev. Lett. **80**, 2602 (1998).
[3] T. Kaneko, Y. Miyahara, R. Hatakeyama, and N. Sato, J. Phys. Soc. Jpn. **69**, 2060 (2000).
[4] I. Funaki, H. Kuninaka, and K. Toki, J. Propul. Power **20**, 718 (2004).
[5] A. Girard, D. Hitz, G. Melin, and K. Serebrennikov, Rev. Sci. Instrum. **75**, 1381 (2004).
[6] T. Suzuki, Y. Sawado, T. Iida, and Y. Fujii, Rev. Sci. Instrum. **75**, 1520 (2004).
[7] N. Itagaki, Y. Kawai, S. Kawakami, and N. Ishii, J. Vac. Sci. Technol. A **20**, 1969 (2002).
[8] M. Tanaka, R. Nishimoto, S. Higashi, N. Harada, T. Ohi, A. Komori, and Y. Kawai, J. Phys. Soc. Jpn. **60**, 1600 (1991).
[9] G. Lisitano, M. Fontanesi, and S. Bernabei, Phys. Rev. Lett. **26**, 747 (1971).
[10] B. McVey and J. Scharer, Phys. Rev. Lett. **31**, 14 (1973).
[11] K. Ohkubo and S. Tanaka, J. Phys. Soc. Jpn. **41**, 254 (1975).
[12] J. Musil and F. Zacek, Plasma Phys. **12**, 17 (1970).
[13] Y. Ueda, H. Muta, and Y. Kawai, Appl. Phys. Lett. **74**, 1972 (1999).
[14] A. Ganguli, M. K. Akhtar, R. D. Tarey, and R. K. Jarwal, Phys. Lett. A **250**, 137 (1998).
[15] T. Kaneko, H. Murai, R. Hatakeyama, and N. Sato, Phys. Plasmas **8**, 1455 (2001).
[16] A. Ganguli, M. K. Akhtar, and R. D. Tarey, Phys. Plasmas **5**, 1178 (1998).
[17] K. Takahashi, T. Kaneko, and R. Hatakeyama, Phys. Rev. Lett. **94**, 215001 (2005).
[18] J. D. Kraus, *Antennas* (McGraw-Hill, New York, 1950), Chap. 7.
[19] D. G. Swanson, *Plasma Waves*, 2nd ed. (IOP, Bristol and Philadelphia, 2003), Chap. 5.